Determination of ultra high-energy cosmic ray composition using surface detector parameters

Marie Lanfermann

Bachelor's Thesis in Physics

Supervisor: Charles Timmermans
July 2012

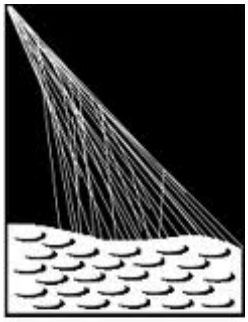

PIERRE
AUGER
OBSERVATORY

Radboud Universiteit Nijmegen

Preface

This bachelor thesis is the result of my Bachelor project at the department of Experimental High Energy Physics of the Institute of Mathematics, Astrophysics and Particle Physics at the Radboud University of Nijmegen.
I would like to thank my supervisor Charles Timmermans, Stefan Grebe, Guus van Aar, Harm Schorlemmer and Stefan Janssen for helping me, teaching me not to go crazy if things do not work out as I want them to and having a nice time.

Contents

Chapter 1

Introduction

1.1 Cosmic rays

Cosmic rays are charged particles that travel through the universe.
We already know that sources of low-energy cosmic rays are stars like our sun. For high energy cosmic rays, with energies of 1PeV and more, we have a few theories from where they may origin. Most of the high-energy cosmic rays are protons. Iron and other heavy atoms can be present too, but their fraction is small when compared to the proton fraction. A class of possible candidates are supernovae but we still do not know. We still have a lot of questions about those high energy cosmic particles.

1. Sources
   We do know that there has to be a source of any sorts. A possible source could be a remnant of a supernova where, because of the high magnetic fields, cosmic particles could be accelerated at astronomical shocks in so called shock acceleration [1] to very high energies, but we do not know this for sure. Another possibility to accelerate cosmic rays are interactions with interstellar clouds [1].

2. Paths
   The interstellar medium in which the cosmic rays are propagating provides numerous possible interactions for the particles depending on their nature. We do not know how to reconstruct the path from the source to Earth because we do not know where every interaction takes place. To learn more about galactic and intergalactic magnetic fields accurate energy measurements are necessary.

3. Interactions in the Earth's atmosphere
   We also do not know all details of the interactions in the atmosphere for

each shower individually The properties of inelastic interactions of nuclei with other nuclei are not known yet exactly. The geomagnetic field also bends the trajects of the rays.

To unravel these issues we perform composition studies on high-energy cosmic rays. This can be done directly with low energy cosmic rays using a sattelite that detects the primary particle. At higher energies an indirect measurement can be performed by detecting the products of the interaction of the cosmic ray with the Earth's atmosphere. Because the flux of high energetic cosmic particles is very low, a sattelite would not be able to detect a significant amount.

1.2 Extensive Air Showers (EAS)

1.2.1 The discovery of Air Showers

In 1939 the French physicist Pierre Auger proposed the existence of air showers. To prove his proposal, he proved a coherence of the air shower particles by measuring cosmic ray events with spaced detectors. He concluded that there was "a small number of coincidences due to air showers" [12] and that with increasing horizontal distance this number decreased quickly within a half meter of the measured maximal signal. For distances of about 10 m a small signal remains. He deduced that the measured particles had to origin from one shower of particles produced in the atmosphere by a primary particle.

When air showers with the energies of primary particles of 10^{20} eV were detected in 1962 it was clear that these particles had to be accelerated by very strong magnetic fields or over very large distances. In fact, the fields had to be so strong (or distances so large) that within our galaxy no such source exists [17]. Therefore, the primary particles of these air showers had to be extra-galactic.
If a charged high energetic cosmic particle with an energy of more than 1 GeV arrives into the atmosphere it sooner or later (depending on the "cross section") collides with a molecule (see figure 1.1). Because of the high energies we are dealing with, the interactions can be described by Quantum Chromo Dynamics (QCD).
The produced particles can either decay, travel to Earth or collide with other molecules. Because the main part of the impulse propagates along the shower axis most of the energy and particles are located near the shower axis. However, the front of the shower is a curved plane, pointing back to a region in which the fastest particles in the front are produced.

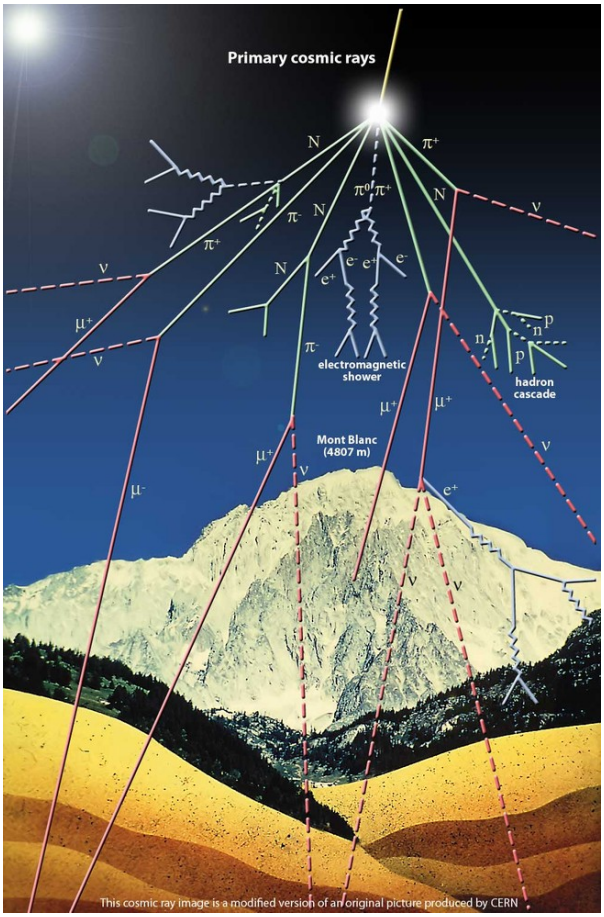

Figure 1.1: A high energetic cosmic particle comes into the atmosphere of the Earth and collides with a molecule. Because of its high energy it can create new particles (secondary particles) that creates new particles or decay. This process creates an Extensive Air Shower (EAS).

The shower of particles that is produced is called an "Extensive Air Shower" or EAS for short.

1.3 The Pierre Auger Observatory

The idea of the Pierre Auger Observatory was to detect high energy cosmic rays with a hybrid detector, meaning two detection strategies being used simultaneous. The two detectors can be used to cross check the results in case both measured the same air shower well. It needed to be built somewhere where the influence of the environment is minimal.
The Observatory has been officially completed in 2008 but has already taken measurements since 2005.

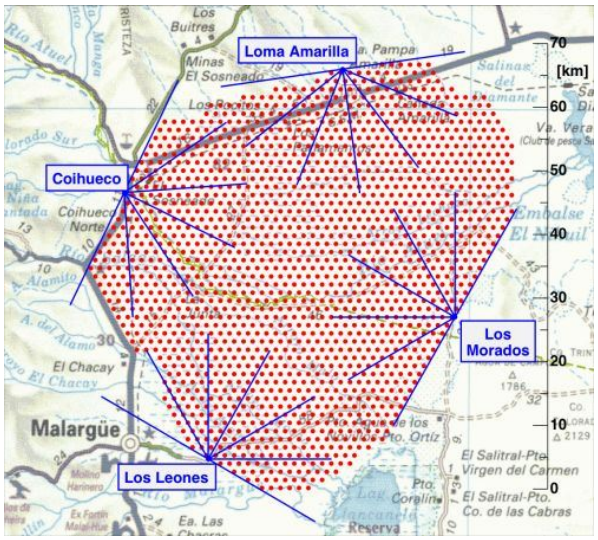

Figure 1.2: Map of the Pierre Auger Observatory. 1600 SD's (red points) are distributed over an area of over 3000 km^2. At the borders of the array 24 FD's oversee the area. The blue lines give the borders of their individual horizontal field of view.

Today the Pierre Auger Observatory consists of about 1600 SD tanks distributed over an area of over 3000 km^2 and 24 FD's distributed over 4 buildings (see figure 1.2).

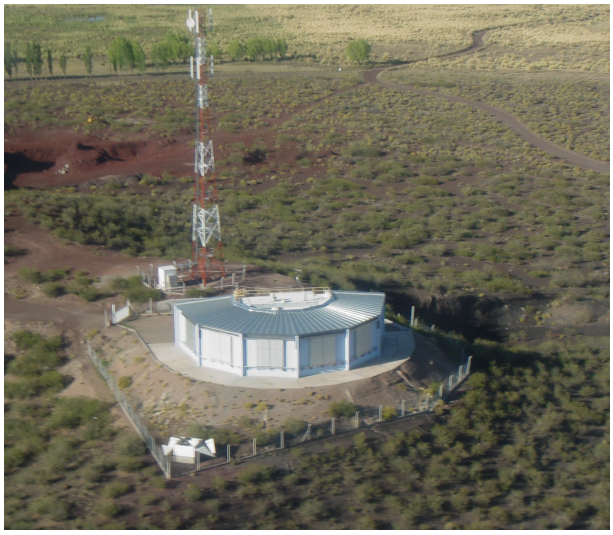

Figure 1.3: Los Leones: One of the 4 buildings containing 6 FD's.

1.3.1 Fluorescence detector (FD)

At the Pierre Auger Observatory 24 fluorescence detectors, or in short FDs, are currently in operation. They are evenly distributed over four buildings (for example Los Leones, see 1.3) that are generally called 'eyes'. In each of these buidings 6 FD's are located. The buildings are arranged in such a way that the FD's view over the surface detectors array.
A FD consists basically of photomultipliers that detect the fluorescence light produced by the high energy particles of the EAS. To make sure that the detectors detect the fluorescence of an EAS. The measurements are taken only in clear moonless nights. We also perform continuous measurements in order to know the what background radiation originating from other light sources in the sky we are dealing with. By using the FD's it is possible to locate the EAS in three dimensions and to estimate where the shower development is maximal. Using atmospheric models we can calculate the amount of atmosphere that the air shower traversed before the maximum number of particles is created. This parameter is called X_{max} and is generally given in g/cm^2. It shall be used a lot in my further analysis. This quantity is the most used quantity to relate to the composition of the primary particle because it is the until now the best understood quantity related to shower development derived from measurements performed at the Auger Observatory.

Figure 1.4: A Surface Detector (SD) behind two cows.

1.3.2 Surface detector (SD)

A surface detector (see figure 1.4), SD for short, consists of a tank containing 12 tonnes of pure water.
Three photomultipliers are located at the top of the inside of the tank. If a high energy particle of an EAS travels through the water in the detector it will produce Cherenkov radiation because of the water's refractive index (n=1.5). This light is emitted in forward traveling direction in a cone that is generally called the Cherenkov-cone. The amount of light is proportional to the number of particles traveling through the tank. By combining the information on particle density and arrival times of all the tanks that were hit by an air shower, the energy and direction of the EAS are reconstructed. The position and timing of every tank is obtained from GPS. Depending on how many stations are triggered, the shower is either classified as small or large.
In my internship I was only interested in larger showers that trigger more than five stations and have an energy of at least 3 EeV. In chapter 2 I will explain the reasons for these criteria.

1.4 Important parameters

Both in the reconstruction of the FD data and the reconstruction of the SD data, a lot of different parameters are constructed that quantify aspects of an air shower. I will now only explain those parameters that are most important to my analysis. First those of the SD followed by the FD.

1.4.1 SD

Zenith angle θ

The zenith angle θ is the angle the angle the shower axis makes with the vertical.

Energy E

The energy of an EAS originates from the energy of the primary particle. This is the sum of their mass energy and their kinetic energy:

$$E = \sqrt{m^2c^4 + p^2c^2}$$

The energy of the primary particle can be estimated from the number of particles at the surface of the Earth.
The energy can also be measured by the FD's, using the total light intensity produced by the air shower. This is a calorimetric approach and has little model dependence.

Radius of Curvature: R_c

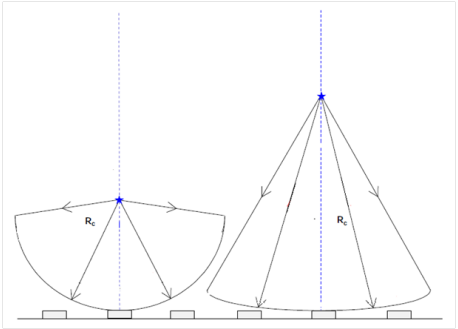

Figure 1.5: The radius of curvature R_c for two different primary particles (left: iron; right: proton) at θ=0.

The Radius of Curvature gives the radius of the showerfront (see figure 1.5). This can be interpreted as the distance between the shower core at the Earth' surface and the point of production of the first particles that readch the surface of the Earth.
The heavier the particle thus the larger its cross section the higher the probability to interact with molecules from the atmosphere and the larger R_c. Lighter particles interact later because of its lower cross section and thus lower probability to interact. This is why, for the same zenith angle θ, showers originating from iron atoms have a greater radius of curvature than those created by protons. Because of geometric reasons it is obvious that R also depends on the zenith angle θ. This has been studied in detail in the Masters thesis of G. van Aar [3].

Risetime: $t_{1/2}$

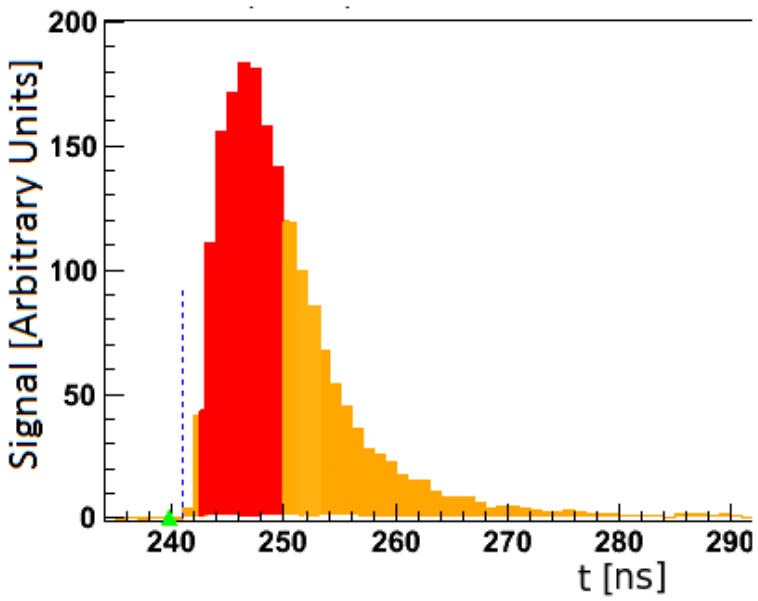

Figure 1.6: The risetime $t_{1/2}$ is the timedifference it takes for the integrated signal to grow from 10% to 50% (red area) of its total integrated signal (orange area).

The risetime is the time it takes for the signal to grow at each surface detector from 10% to 50% of the total integrated signal (see figure 1.6).

1.4.2 FD

Slanth depth: X_{max}

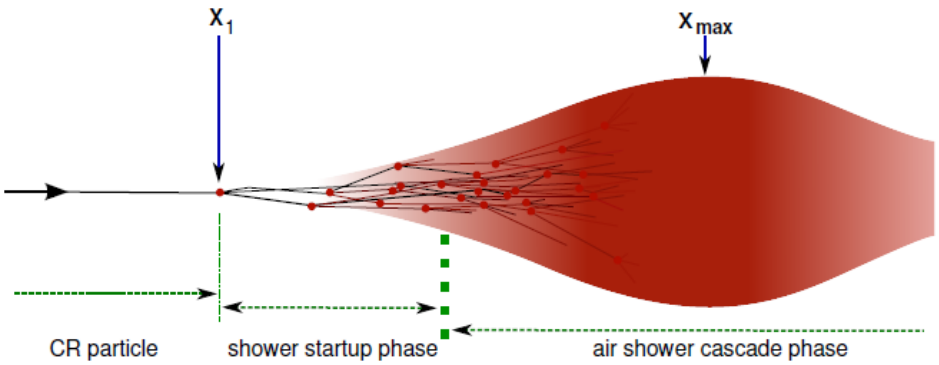

Figure 1.7: The FD parameter X_{max} [4] is indicating the amount of atmosphere the particles of the EAS propagated through until the number of produced particles is at its maximum..

The parameter X_{max} gives the amount of atmosphere a shower traversed before the maximum particle density is reached (see figure 1.7). It is calculated from the measurement of the amount of fluorescence light and the corresponding position of an EAS. An atmosphere model is used to convert altitude to an amount of atmosphere.

1.5 Motivation

The FD parameter X_{max} is until now the best understood and most precise parameter related to the composition of the primary particle. But the downside of using this parameters is that X_{max} is a parameter measured by the FD and therefore can only be measured at cloudless nights. The fact that the FD can only measure 10% of the total time effects the quantity of the measurements. Having only few measurements of this parameter restricts studies about the composition of the primary particle. It would be really helpful in the research of ultra high energy cosmic particles if there was a way to determine X_{max} out of SD data.

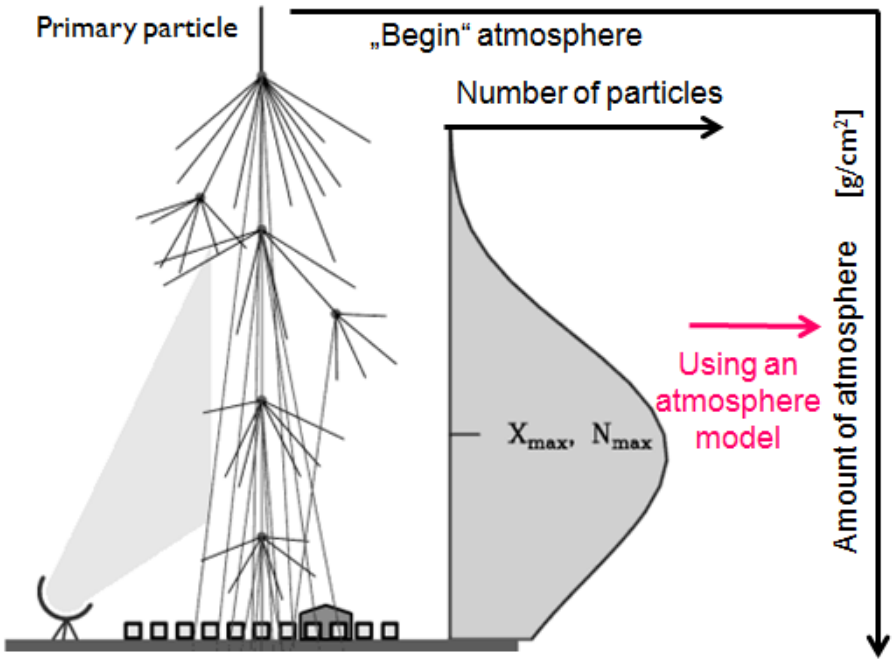

Figure 1.8: The FD parameter X_{max} is measured using a atmosphere model.

In my bachelor project I looked for a way to get an average X_{max} calculated from SD data. To figure out which combination of parameters is the best, requires a high quality SD data set. After the event selection, I correlate the SD parameters with the FD parameters, by using events where both FD and SD measurements exist.
I will search for dependencies in parameters of interest and obtain the correlations between X_{max} and the SD parameters R and $t_{1/2}$. Afterwards I will combine the SD parameters to an unphysical parameter to strengthen the correlation.

Chapter 2

Selection Criteria

In order to get a high quality set of EAS, I designed a set of selection criteria. These criteria judge the quality of two data sets. One set of selection criteria are used for the FD data and one for the SD data.
All used selection criteria and the corresponding ADST code are listed in Appendix A.

2.1 FD selection criteria

The criteria with which I select the FD data are mentioned below.

Reconstruction levels

Before considering the quality of the reconstruction of a shower we need to make sure that all events that are to be considered are of sufficient quality.
The FD measurements have to contain a reconstruction of X_{max}.
For this analysis I choose the highest quality reconstruction level, up to an energy estimate.

Station Axis distance

The distance between the shower axis of the EAS and the hottest station should be less than 2 km. A similar selection cut will be discussed in the SD selection but in this case the shower axis as determined from the FD data is being used.

Clouds

Clouds can block fluorescence radiation and therefore influence the FD measurements. Measurements that were taken during cloudy nights might have a

large systematic bias as we do not know if all light of the EAS arrived at the fluorescence detectors unblocked or if there was a cloud in between shower and detector blocking a (large) fraction of the fluorescence light. The LIDAR system provides information related to the amount of clouds and their distance to the ground [14]. The term LIDAR stands for LIght Detection And Rangings.
I decided to select only events that have LIDAR data and where no clouds are present.

Cherenkov radiation influence

Cherenkov radiation occurs if a high energetic particle, that moves at relativistic velocities, travels at group velocity $v_g > \frac{c}{n}$ through a medium of refractive index n>1. The refractive index of air at sea level is equal to 1.0003 [1].
Cherenkov light contaminates the fluorescence signal [7]. When there is too much Cherenkov radiation in the FD measurements, the energy and the X_{max} measurement can be influenced.
For these reasons, I included the selection of having at most 50% of Cherenkov radiation in the FD measurements.

Is X_{max} within the field of view?

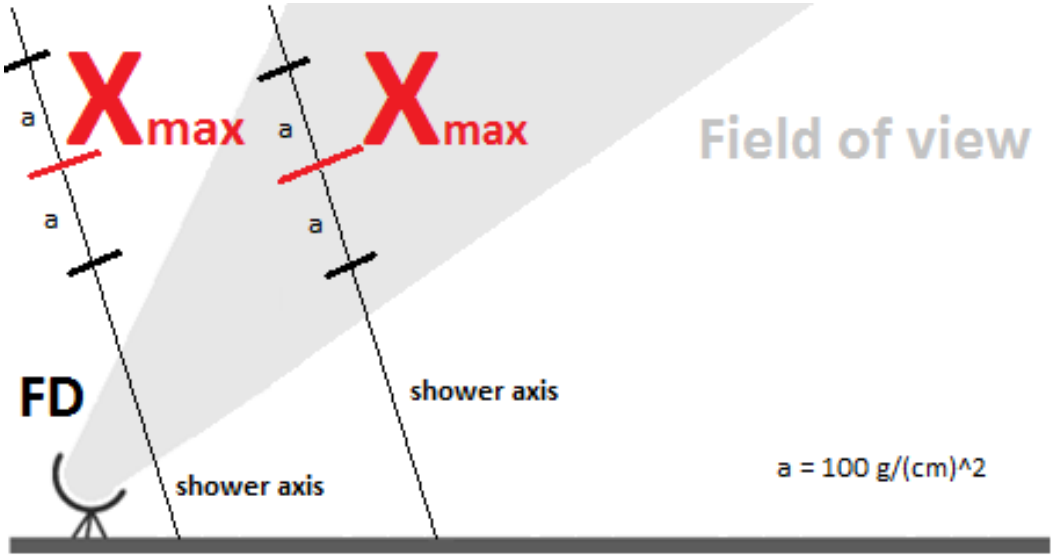

Figure 2.1: Assuming the same primary particle at the same energy, the same shower development and shower axis the quality of reconstruction also depends on whether X_{max} is in the field of fiew or not.

Each FD has a field of view of 30 by 30 degrees. Therefore, it can only detect fluorescence light in a certain area. One might compare it with an eye. Near the FD only a part of the shower created by high energy cosmic rays near ground can be detected while at some distance away from the FD it is possible to detect light created by showers further up in the atmosphere (see figure 2.1). So if the primary particle were an iron atom it would not be measured correctly by the FD station if its EAS came down too close to it. Only the tail of the EAS would be detected which makes it impossible or at least hard to reconstruct it and examine the X_{max} value. This is why it is important to know if the maximum of the shower development was indeed seen by the FD. It is also the reason I added the selection criteria of X_{max} having to be in the field of view of the FD taking the measurements.
Considering the fact that X_{max} should be in the field of view, it is important that the measured X_{max} does not lie at the border of the field of view but a certain distance away from that border. From studies in the EventBrowser I decided that the X_{max} not only needs to be in the field of view, but that the boundary of the field of view should at least be 100 g/cm^2 away from X_{max}. This ensures a proper fit of the shower shape and provides a good resolution on the individual measurements of X_{max}.

Difference in the χ^2 value between Gaisser-Hillas fit and linear profile fit

The FD measurements can be described by the empirically proven Gaisser-Hillas (GH) function [6]:

$$f_{GH}(X) = N_{max}\left(\frac{X - X_0}{X_{max} - X_0}\right)^{\frac{X_{max}-X_0}{\lambda}} e^{\frac{X_{max}-X}{\lambda}}$$

The Gaisser-Hillas function is the function which determines X_{max}. In this function X_0 and λ are fit shape parameters. The energy dependent parameter X_0 is weakly correlated with the shower start but does not have a physical meaning and λ is the mean interaction length.
In case of an EAS whose shower core lies in the SD array it is necessary that the FD measurements resemble a GH function better than an linear profile fit. One way to check this behaviour is to determine the χ^2-agreement between the data and both functions, and substract these χ^2 values. Again, by studying events in the EventBrowser, a minimal χ^2 difference of 10 seemed appropriate. Example profiles are shown in figures 2.2 to 2.7.

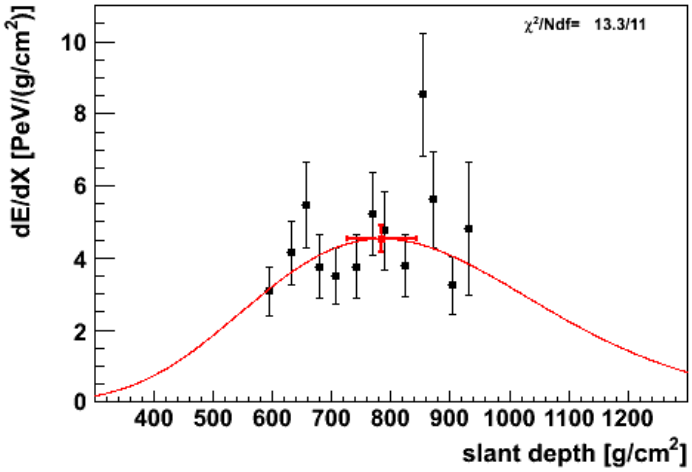

Figure 2.2: FD measurements with a χ^2 difference between GH and linear profile fit of 0.8.

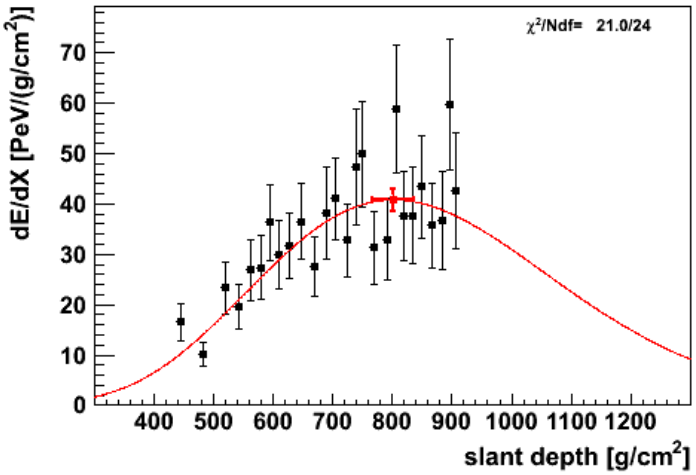

Figure 2.3: FD measurements with a $\chi 2$ difference between GH and linear profile fit of 4.5.

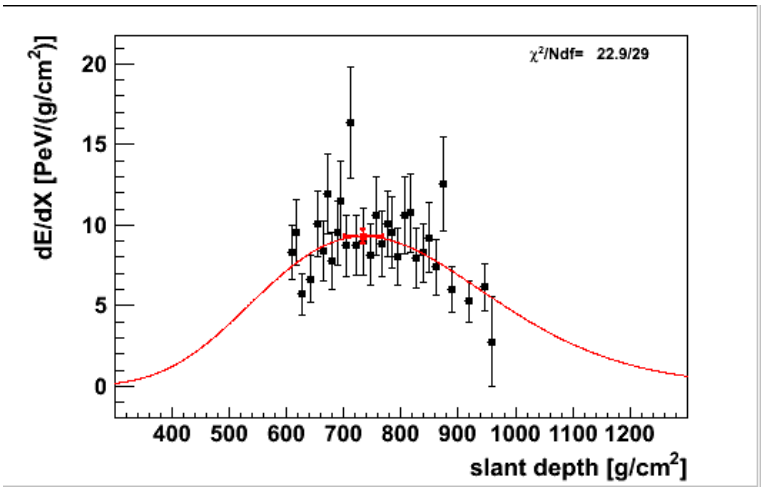

Figure 2.4: FD measurements with a $\chi 2$ difference between GH and linear profile fit of 10.7.

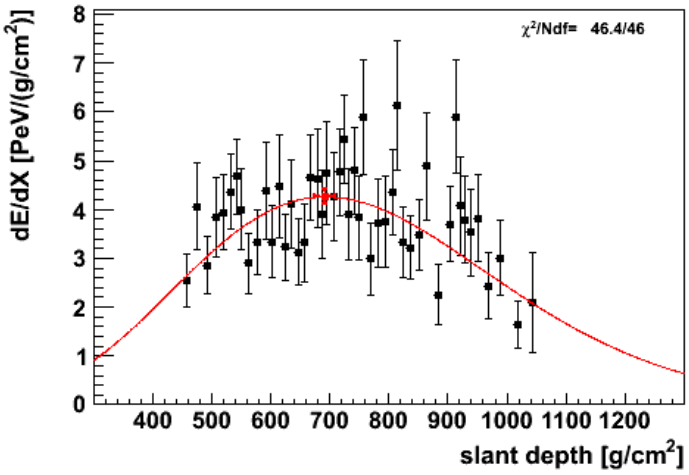

Figure 2.5: FD measurements with a χ^2 difference between GH and linear profile fit of 17.2.

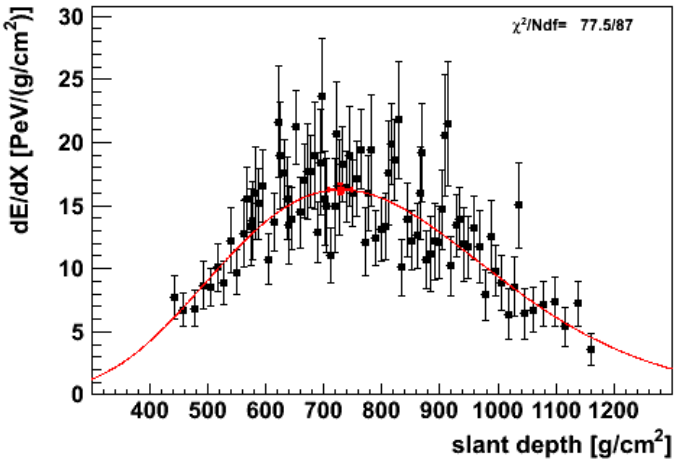

Figure 2.6: FD measurements with a χ^2 difference between GH and linear profile fit of 182.0.

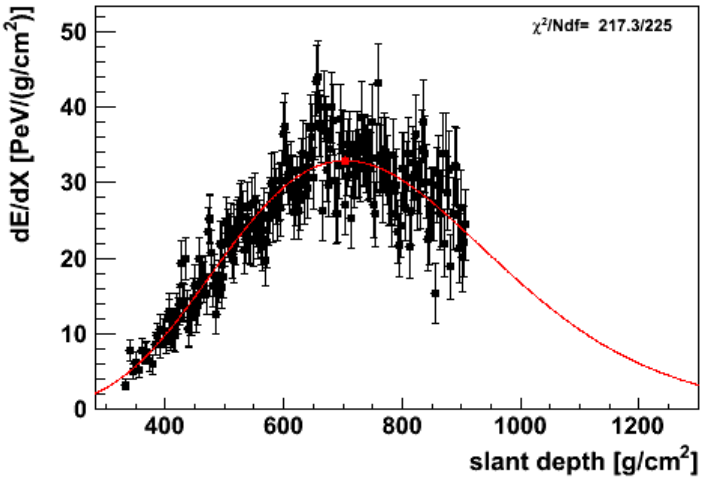

Figure 2.7: FD measurements with a χ^2 difference between GH and linear profile fit of 496.1.

Events measured by more than one eye

As there are 4 different buildings with fluorescence detectors at the Pierre Auger Observatory, it is possible that several eyes can detect fluorescence light of an EAS. The reconstruction of the data of each eye will be of a different quality, depending on the amount of light detected and the geometry of the air shower. This is why I decided to take all of the X_{max_i} values for all eyes that fullfill all selection criteria into account, average them and weigh their importance according to their individual uncertatinty σ_i.
For this I used the weighted mean value of X_{max}:

$$X_{max} = \frac{\sum_{i=1}^{N_{Eye}} \frac{X_{max_i}}{\sigma^2_{X_{max_i}}}}{\sum_{i=1}^{N_{Eye}} \frac{1}{\sigma^2_{X_{max_i}}}}$$

Number degrees of freedom (ndf) of the Gaisser-Hillas (GH) fit

The ndf originates from the number of measurements and restrictions:

$$\text{ndf} = \#(\text{measurements}) - \#(\text{restrictions}) \tag{2.1}$$

The GH fit should at least have a ndf of one. Otherwise there are not enough measurements to draw accurate conclusions.

χ^2/ndf of the GH fit

To select only events that are in good agreement with the expectations I decided to make a cut on the value of χ^2/ndf that indicates the deviations of the measurements to the fitted functions with respect to their uncertainties.
Fo this I used the FD selection criteria explained up to now and the SD selection criteria explained in the next section up to the maximum value for the χ^2/ndf for the LDF and AF which will be eplained in the next section, too.

The maxiumum value I decided to allow for χ^2/ndf of the GH fit is 1.4625. This cut removes 10% of the events with the worst fits of the shower shape (see figure 2.8).

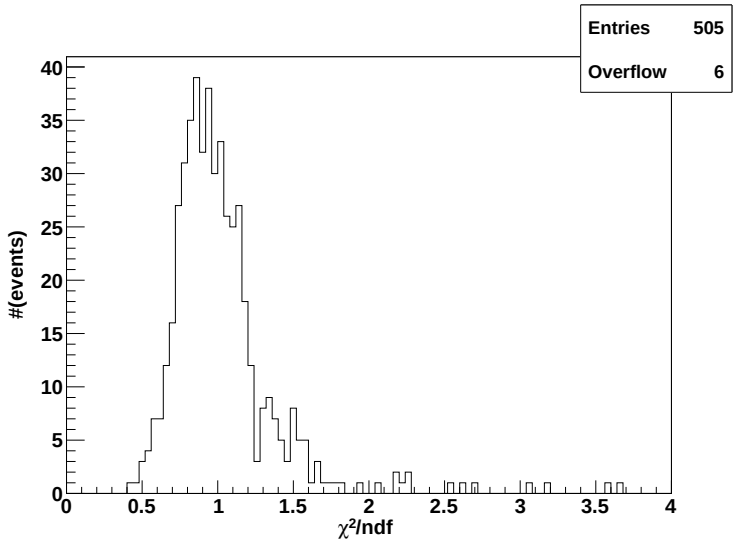

Figure 2.8: The distribution of the χ^2/ndf value for the GH fit. Cutting away the highest 10% means a maximum allowed value of 1.4625.

2.2 SD selection criteria

The basic SD cuts I made to the data are listed below.

Reconstruction levels

We want the SD measurements to provide an energy and a three dimensional direction of the EAS. Each of these parameters adds to the reconstruction level, which is why the reconstruction level of the SD events has to be at least 4.

Minimum number of triggered stations

An event should at least have triggered 5 stations to be considered in this study. This is needed in order to properly measure the radius of curvature from the SD information.

Number degrees of freedom ndf

The number degrees of freedom is calculated from the amount of restrictions in a fit and the number of measurements used in that same fit (see equation (2.1)). In this work, the following fits are used:

- Lateral Distribution Function (LDF)
  The LDF describes the particle density as a function of the distance of the point of measurement (SD) to the shower axis [13].

- Angle Function (AF)
  The angle function (AF) (see equation 2.2) is the SD plane fit [10] where the shower is approximated by planes perpendicular to the shower axis. The AF describes the impact time of the shower particles on the ground t($\vec{x}$) with respect to the estimated time t_0 of the arrival of the shower front at the shower core at the barycenter $\vec{b}$. The unit vector $\hat{a}$ points along the shower axis toward the origin of the shower.

$$ct(\vec{x}) = ct_0 - (\vec{x} - \vec{b})\hat{a} \tag{2.2}$$

- Risetime fit
  The risetime $t_{1/2}$ is measured by each SD station triggered by the EAS individually. Because the stations are placed at different distances with respect to the shower axis, an empirically determined function is fitted to these measurements from which $t_{1/2}$ at a distance of 1000 m is determined. This value can be compared for all measured air showers.

Just like before with the GH fit all these fits should have at least one degree of freedom. The reasons are the same as in the previous case.

Zenith angle θ

As mentioned earlier, θ is the angle between the shower axis and the vertical. Because reconstruction gets complicated if the zenith angle of an event gets close to 90° it is convention to consider only events up to an maximal zenith angle of 60°.

Energy

Air showers with energies below 3 EeV are rejected because the array is only fully efficient for EAS with higher energies. The range of energies for my set of cosmic rays is then from 3 EeV to 100 EeV (see figure 2.9).

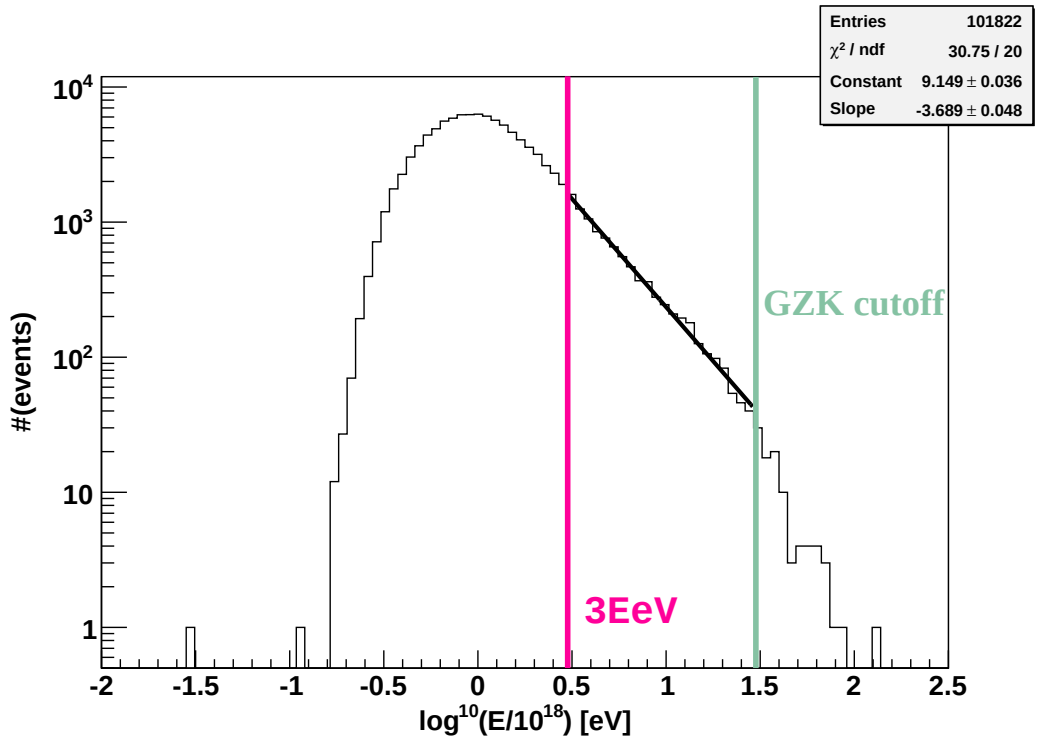

Figure 2.9: Energy distribution of high-energy events measured by SD's and FD's. Only the selection criteria on the reconstruction levels are taken into account.

For energies above 30 EeV there are far less events than one might expect when extrapolating the flux from the lower energies. This sudden lack of events could originate from the GZK cutoff [11] where cosmic rays interact with the cosmic background radiation.
The reconstruction for energies below 3 EeV does not always work well enough and the Observatory is not suited to measure these showers as well as it reconstructs those above this energy.
Considering only energies above 3 EeV we get an almost linear correlation between ln(N) and $\log_{10}$(E) (see equation 2.3), so it follows that the number of events is similar to E^a (see equation 2.4).

$$log(N) = a \cdot log^{10}(E) + b \tag{2.3}$$
$$\Rightarrow N \propto E^a \tag{2.4}$$

For this data set, taking all basic cuts except the 6T5 trigger into account, the value of a is -3.689 $\pm$ 0.048 events/EeV.

This corresponds to a γ of 2.689±0.048. The literature value of γ for this energy range is 2.65±0.14 [18] so the two values are in agreement with each other.

Quality trigger (T5): 6T5

The quality trigger 6T5 selects only those events that have an excellent energy reconstruction and arrival direction reconstruction. The core position of the EAS must be inside the limits of the SD array.
This cut ensures that you do not classify a big EAS, whose core position is a few km away from the SD array and triggers some SD's on the boundary of the array, as a small event. The 6T5 trigger selects only events where all of the 6 closest neighbours of the SD station in the hexagonal SD array which detected the largest signal are existing and operating. The shower core must be reconstructed in the area between these stations (see figure 2.10).

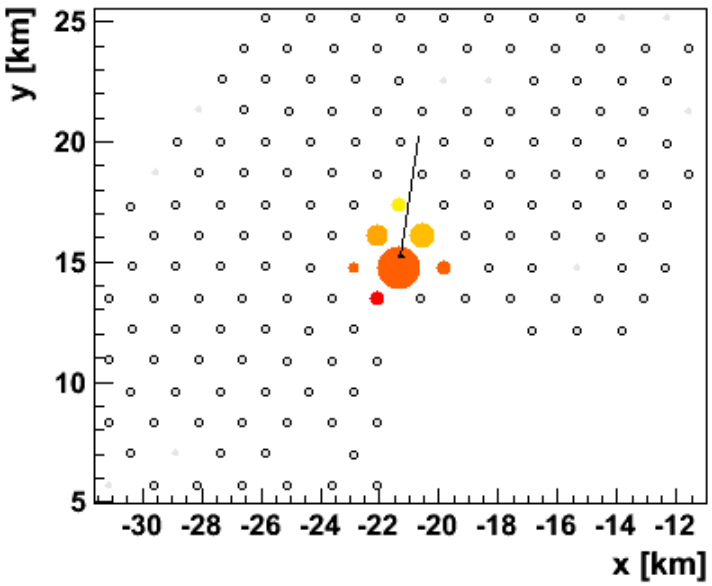

Figure 2.10: Each circle corresponds to a SD of the SD array. The triggered SD's are coloured according to the time of triggering from yellow to red. The radius of the colouring indicates the amount of Cherenkov light produced by the EAS in the SD. The 6T5 trigger requires for all six SD's around the station where the most Cherenkov light has been produced exist and are functioning.

For the purpose I intend to use the data a good measurement of X_{max} is crucial. So therefore I chose to add the 6T5 trigger to the data selection criteria.

χ^2/ndf of the LDF and AF

Cutting away 10% of the measurements (for their distribution see figures 2.11 and 2.12) with the highest χ^2/ndf value for both functions improves the quality of the set of selected events.

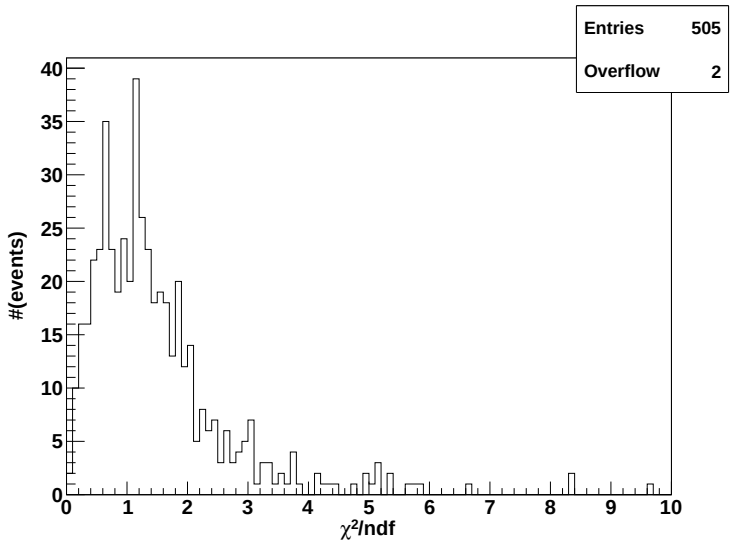

Figure 2.11: The measurements of χ^2/ndf of the LDF.

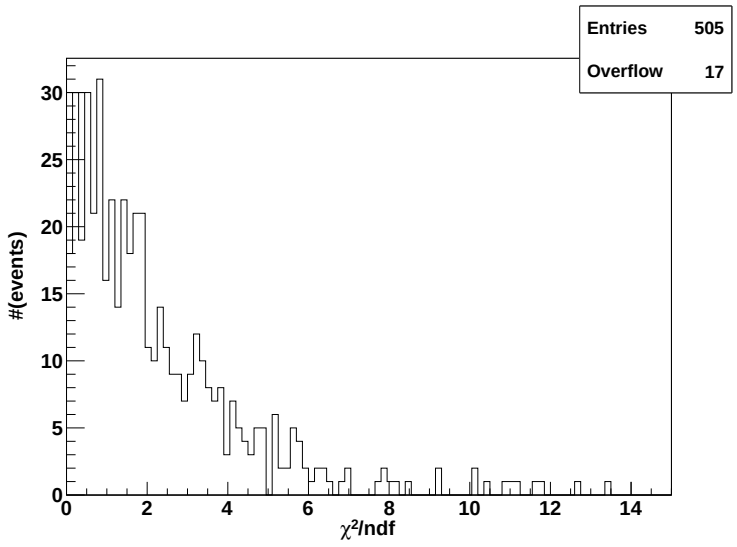

Figure 2.12: The measurements of χ^2/ndf of the AF.

The precise values of the χ^2/ndf limits are listed below.

Detector	Fit	Highest allowed value of χ^2/ndf
SD	LDF	3.05
	AF	5.775

The histogram for the AF shows a lot of events that have a χ^2/ndf of nearly zero. This is highly unlikely for a proper χ^2 distribution.

Relative error of E

It is for obvious reasons important that the error on the energy does not become too large.

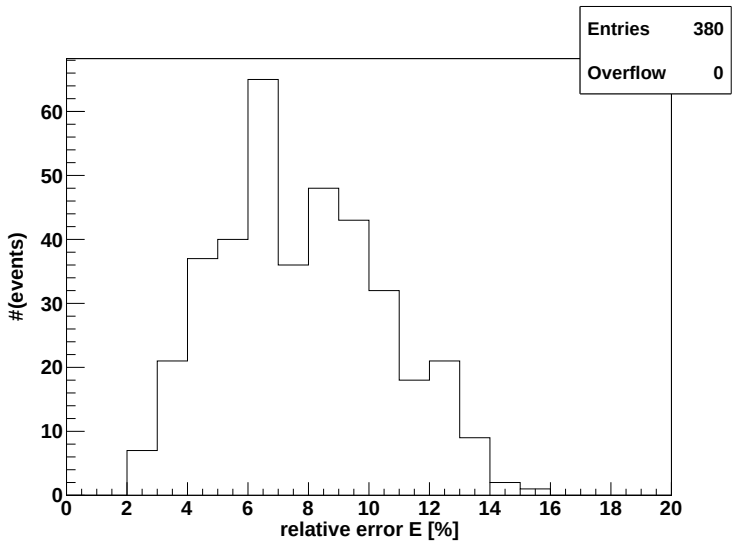

Figure 2.13: The relative error on the energy E. Making the cut at 13% seems appropriate.

Considering the distribution of the relative energy error (see figure 2.13) the maximum allowed value for a relative error on the energy is 13%.

Relative error of the radius of curvature R

Considering the distribution of events with respect to the relative error of R a maximal relative error of 30 % seems appropriate (see figure 2.14).

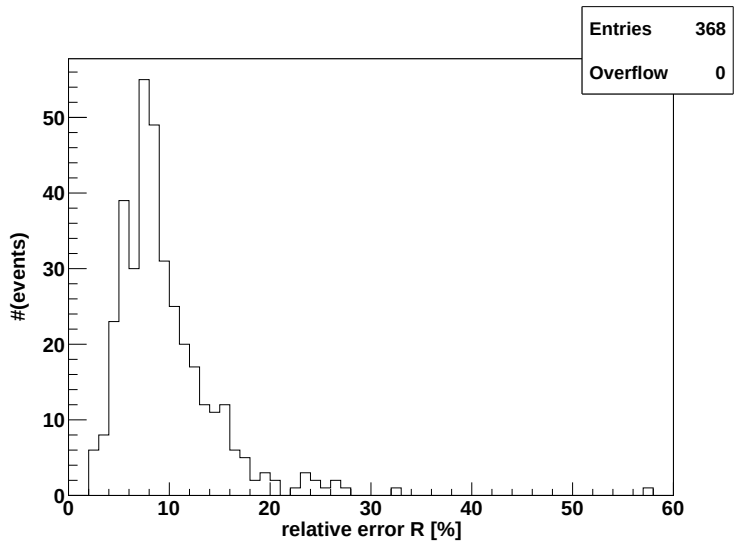

Figure 2.14: The relative error on the radius of curvature R. Making the cut at 30% seems appropriate.

Risetime $t_{1/2}$ cannot be zero or less

A negative risetime is physically not possible. So the first thing to demand on the risetime is for the value to be higher than zero. Another important point is that the ndf of the $t_{1/2}$ fit has to be at least one.

Relative error $t_{1/2}$

Because of the earlier mentioned calculation of $t_{1/2}$(1000 m) the error is uncertainty is rather high. Therefore considering the distribution of events (see figure 2.15) the error should be less than 100%.

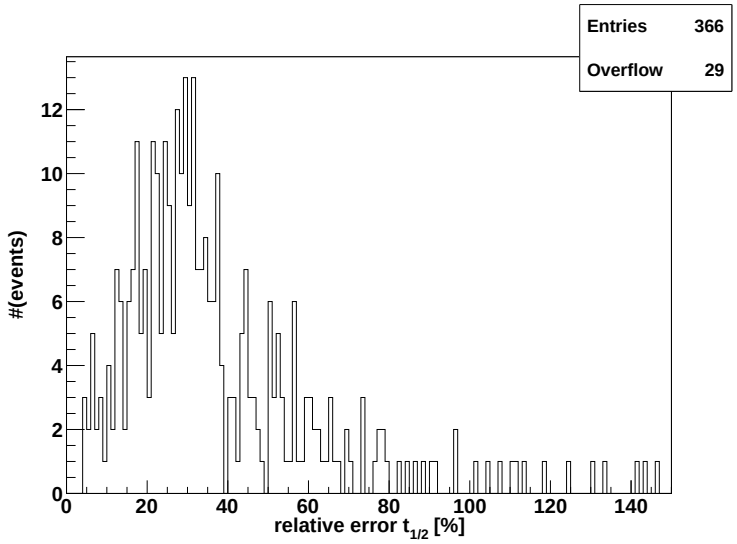

Figure 2.15: Considering the calculation to get $t_{1/2}$ at a certain distance to the shower axis the relative error is quite high. Considering only events with an relative error of less than 100% seems appropriate.

χ^2/ndf of the $t_{1/2}$ fit

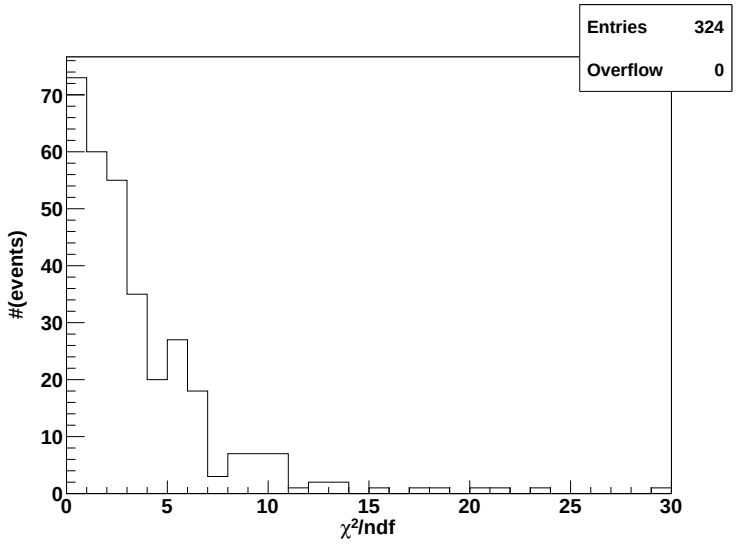

Figure 2.16: The measurements of $t_{1/2}$ vary a lot from the empirically proven function because of the calculation for 1000 m distance.

Considering the distribution of values of χ^2/ndf for the $t_{1/2}$ fit (see figure

2.16) it seems appropriate to make the cut at a value of 10.

2.3 The set of events to be used in the correlation studies

Including all these selection criteria on all up to now measured Golden Events a set of 324 ADST events remains on which I will base my correlation studies.

Chapter 3

Correlation studies

I will first discuss the correlation studies of R - X_{max} and later of $t_{1/2}$ - X_{max}. Then I will combine these two parameters to $t_{1/2}$/R and check the correlation with X_{max} to see if it is indeed possible to calculate an X_{max} from this. To check this I will use the energy dependency of X_{max} and compare it with actual measurements using the same ADST files.
In the correlation studies I propagated errors according to the method shown in Appendix B.

3.1 R - X_{max} correlation studies

In order to obtain the correlation between R and X_{max} I first checked if these parameters had any other dependencies. In case there were any, I corrected them before studying the pure correlation between R and X_{max}.

Zenith angle θ dependency of R

Earlier studies [8] showed that the radius of curvature depends on the zenith angle θ (see equation (3.1)).

$$R_c = R \cdot \cos(\theta)^{\alpha(E)} \tag{3.1}$$

$$\alpha(E) = (1.318 \pm 0.056) + (0.11 \pm 0.11)\log(E) + (-0.125 \pm 0.055)(\log(E))^2 \tag{3.2}$$

This correction will be used in the following analysis.

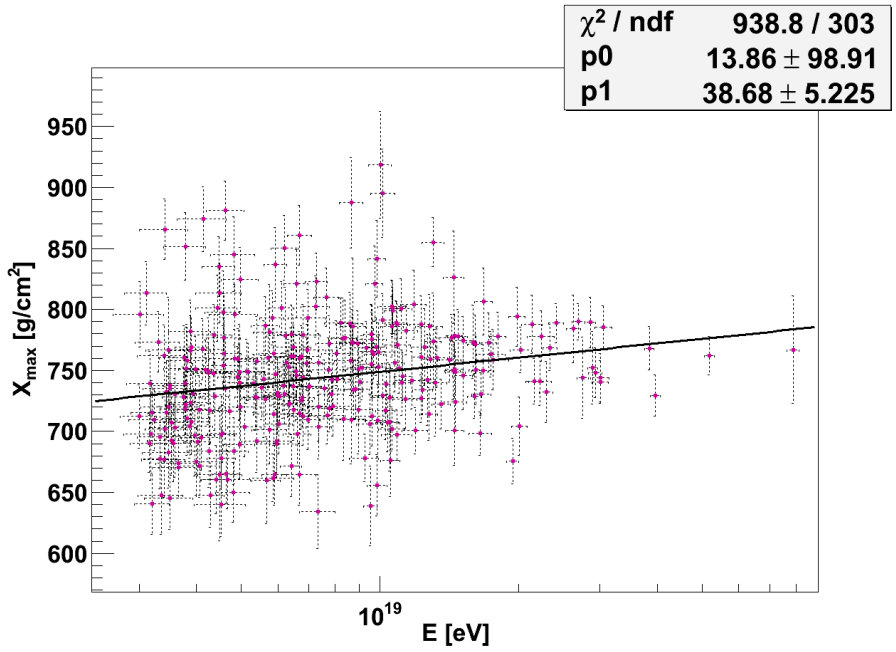

Figure 3.1: The correlation between the energy E and X_{max} with a correlation facor of 0.17.

Energy dependency of X_{max}

The energy dependency of X_{max} is shown in figure 3.1.
I choose all my corrections to be such that the average value I am correcting to is 750. In this case, at an energy of 10.7 EeV, the average value of X_{max} is 750. Therefore, I correct the Xmax to the corresponding value at an energy of 10.7 EeV. In log10 scale this corresponds to 19.03 (see equation (3.3)). I wil use this value again to correct R_c to get R_{corr} (see equation (3.4)).

$$X_{max,c} = (38.68 \pm 5.23) \cdot (19.03 - \log_{10}(\frac{E}{eV})) + X_{max} \tag{3.3}$$

Comparing the elongation rate of 38.68 ± 5.23 g/cm^2/decade to the elongation rate of 27^{+3}_{-8} g/cm^2/decade as found in earlier studies [15], it is obvious that the elongation rate I evaluated is much higher. However, this dataset is best described by it. The reason for the deviation might be in corrections applied at low energies in order to correct for the FOV of the fluorescence detector. In general, that would increase the average Xmax value at low energy, and therefore decrease the elongation rate. This does require more research though. In this work, it is assumed that although, due to the selection criteria we might have a biased dataset, biases will be the same in the SD and FD parameters. In

other words, the correlation between the parameters is not influenced by these biases.

Energy dependency of R

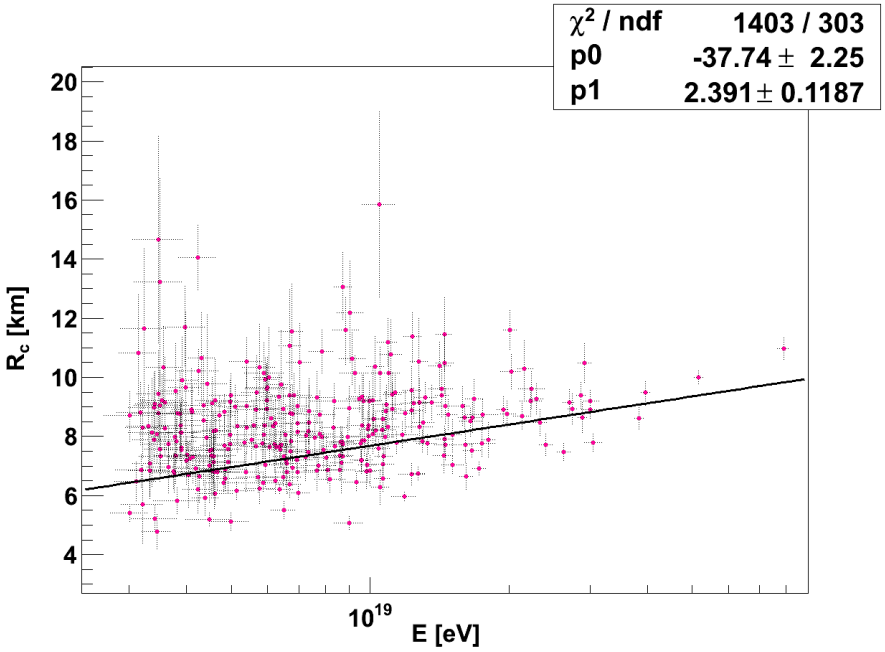

Figure 3.2: The correlation between the energy E and R_c with a correlation factor of 0.29.

The energy dependency of R_c (see equation (3.4)) is shown in figure 3.2.

$$R_{corr} = (2.39 \pm 0.12) \cdot (19.03 - \log_{10}(\frac{E}{eV})) + R_c \tag{3.4}$$

After all these dependencies are taken out of the equation, the actual correlation between R and X_{max} is shown in figure 3.3.

$$X_{max,c(R)} = (-28.57 \pm 2.48) \cdot (8.35 - R_{corr}) + X_{max,c} \tag{3.5}$$

This correlation is now independent of the energy correlation of both parameters. Only a mild correlation is found. This could be due to the fact that the correlation varies as a function of energy, or that the reconstruction quality is not good enough to get a better correlation. Another possibility is that these parameters are truly only weakly correlated in nature. Choosing between these options requires more study.

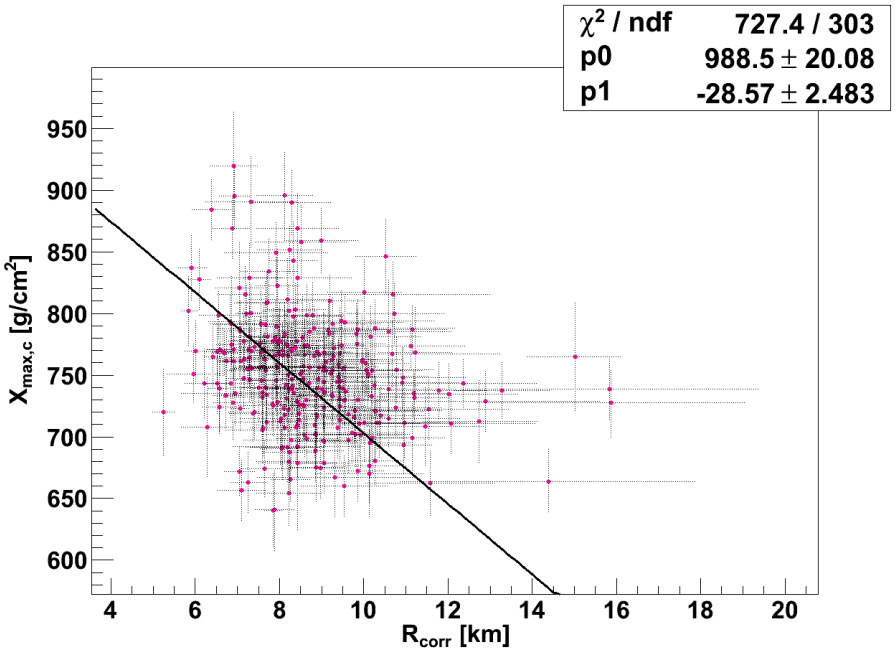

Figure 3.3: The correlation between the R and X_{max} with a correlation facor of -0.24.

3.2 $t_{1/2}$ - X_{max} correlation studies

Zenith angle dependence on $t_{1/2}$

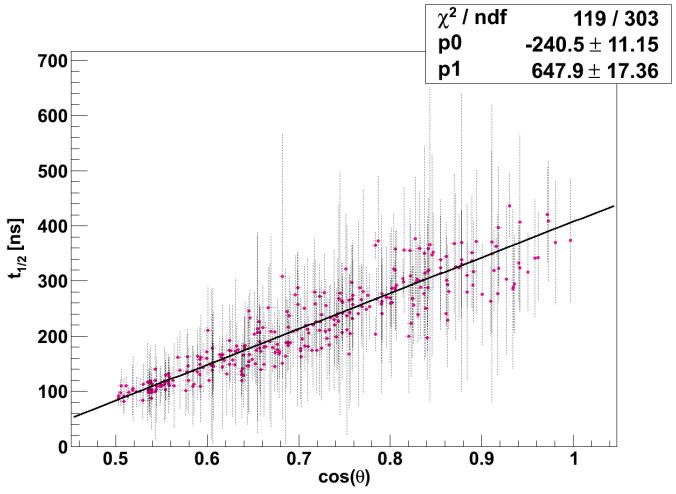

Figure 3.4: The correlation between θ and $t_{1/2}$ with a correlation facor of 0.92.

As mentioned earlier, most particles of an EAS are near the shower axis, so the "thickness" of an EAS decreases with increasing distance to the shower axis. To be able to compare the risetimes of events with different zenith angles, their $t_{1/2}$ value is being corrected with respect to $\cos(\theta) = 0.75$ which corresponds to an zenith angle of 41.4° (see equation 3.6). The distribution of $t_{1/2}$ with respect to $\cos(\theta)$ can be seen in figure 3.4.

$$t_{1/2,c} = (647.9 \pm 17.36) \cdot (\cos(\theta) - 0.75) + t_{1/2} \tag{3.6}$$

Energy dependency of $t_{1/2}$

No energy dependence of $t_{1/2}$ was found when using an event energy estimator based on the number of particles at 1000 metres for each event.

The correlation between $t_{1/2}$ and X_{max}

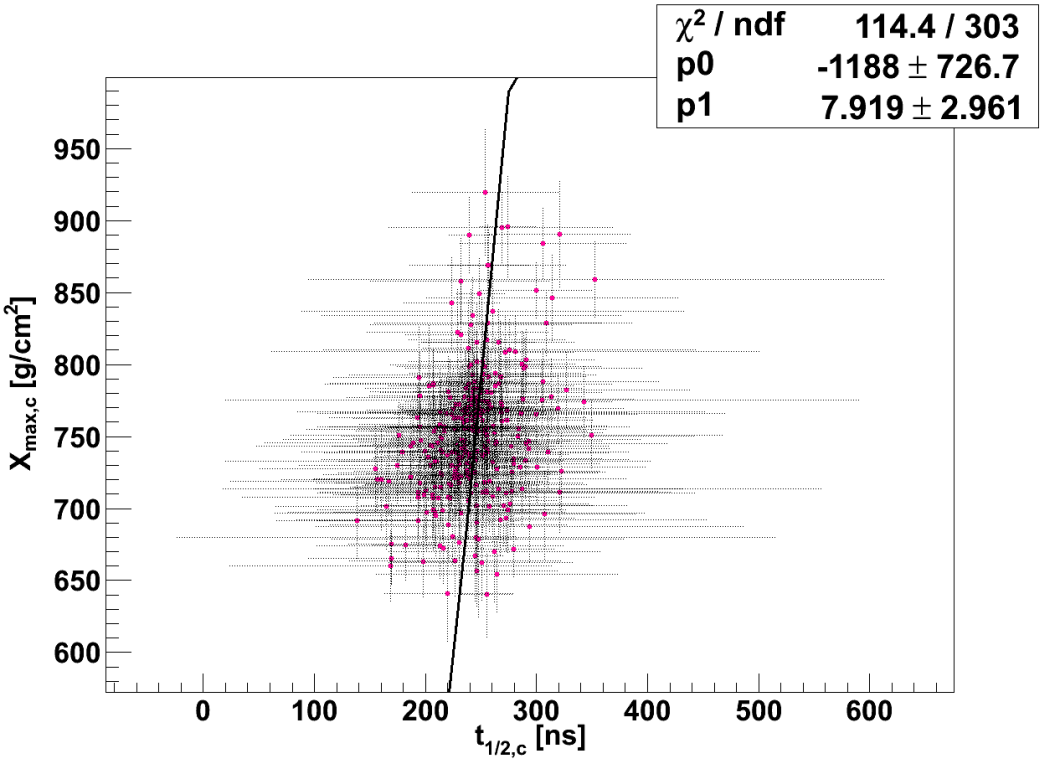

Figure 3.5: The correlation between $t_{1/2,c}$ and X_{max} with a correlation facor of 0.32.

Even though the correlation between $t_{1/2}$ and X_{max} (see figure 3.5) is weak, its correlation factor is only 0.32, a correlation between these two parameters

is expected. Again, calculating an X_{max} with respect to the corresponding $t_{1/2}$ value of 244.73 corresponding to 750 g/cm^2 leads to equation 3.7 as an equation for an $t_{1/2}$ corrected value for X_{max}.

$$X_{max,c(t_{1/2})} = (7.92 \pm 2.96) \cdot (244.73 - t_{1/2,c}) + X_{max,c} \tag{3.7}$$

3.3 Combined $\frac{t_{1/2}}{R}$ - X_{max} correlation studies

If both SD parameters R and $t_{1/2}$ are combined to $t_{1/2}/R$ a stronger correlation with X_{max} is found, even though this is independent on any physical importance of this combination of parameters. In the earlier correlations the correlation factors were -0.24 (see figure 3.3) and 0.32 (see figure 3.5) while in the case of combined SD parameters the correlation factor is 0.42 (see figure 3.6)

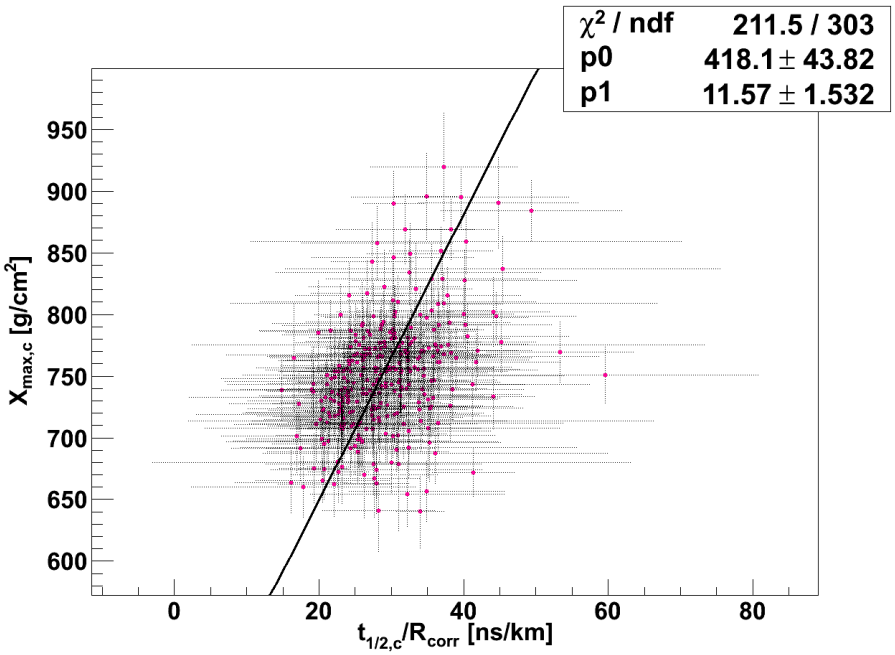

Figure 3.6: Correlation between $t_{1/2,c}/R_{corr}$ and X_{max} with a correlation factor of 0.42.

$$X_{max,c(t_{1/2}/R)} = (11.57 \pm 1.53) \cdot (28.69 - t_{1/2}/R_{corr}) + X_{max,c} \tag{3.8}$$

From the earlier R - X_{max} and $t_{1/2}$ - X_{max} correlation studies it is possible to calculate the expected slope of this correlation as shown in Appendix B.2. The expected slope is 7.4. This could be due to the fact that some of the effects

reducing the correlation in the earlier analyses are compensated, and therefore not only the correlation coefficient increases, but also the dependency becomes stronger.

Chapter 4

Results and Conclusion

Even though the correlation is weak it is possible to estimate X_{max} from the SD data.
Because of the weak correlations the dependency of the combined parameter is different from the calculations using the individual parameters. This makes the results less credible.

To check the results one might for example check the energy dependency of the X_{max} measured by the FD (see figure 4.1) with the energy dependency of the calculated X_{max}.

Checking the energy dependency on X_{max}

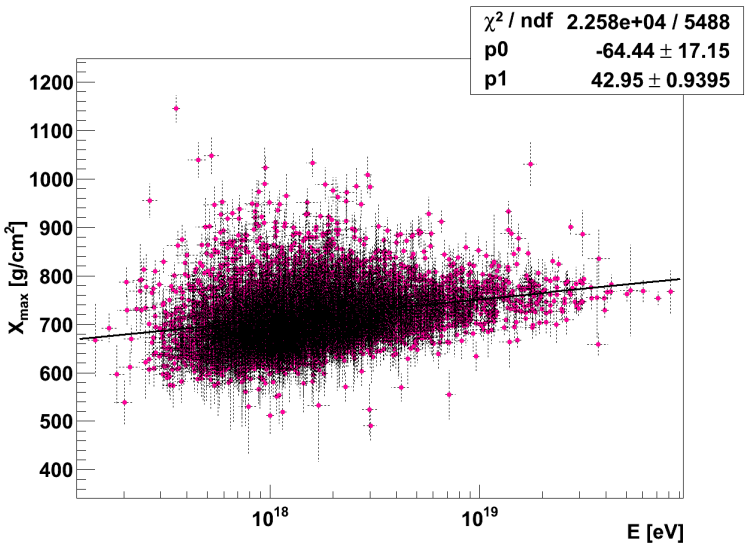

Figure 4.1: The energy dependency of X_{max} measured by FD's.

The literature value of the elongation rate of 27^{+3}_{-8} g/cm^2/decade [15] is not in agreement with the elongation rate resulting from the (uncorrected) FD measurements as seen in figure 4.1, where we find 43.0±0.9 g/cm^2/decade. These values are uncorrected, which causes a bias especially at low energies.
Using R to calculate X_{max} (see figure 4.2) gives an elongation rate of 108.7±1.5

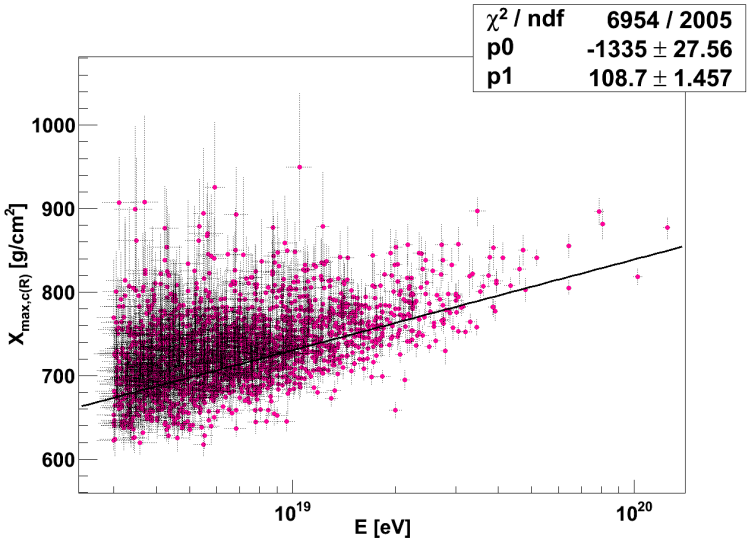

Figure 4.2: The energy dependency of the calculated X_{max} using the SD parameter R.

g/cm^2/decade that neither fits the literature value nor the value calculated by the FD measurements.
From this analysis, the SD parameter R alone does not seem to be a reliable parameter to calculate an X_{max} from SD data.
As can be seen in figure 4.3 some values of $X_{max,c(T)}$ are zero or even negative. This cannot be physically possible but is a result from the large slope found in 3.5 which is used in the correction. The elongation rate found in earlier studies and the elongation rate found in the FD measurements are both within the uncertainty of the elongation rate found in this analysis 40±26 g/cm^2/decade, but only because of large uncertainties of $X_{max,c(T)}$. This large uncertainty arises from the combination of a general large uncertainty on the risetime in the ADST files and a large slope from figure 3.5, which increases the error on the calculated values of $X_{max,c(T)}$.
So, using this analysis, the SD parameter $t_{1/2}$ is not a accurate parameter to calculate an X_{max} from SD data. Using the combination $t_{1/2}$/R (see figure 4.4) leads to an elongation rate of 23±7 g/cm^2/decade which is nearer to the elongation rates from the FD measurements and, when compared to the literature

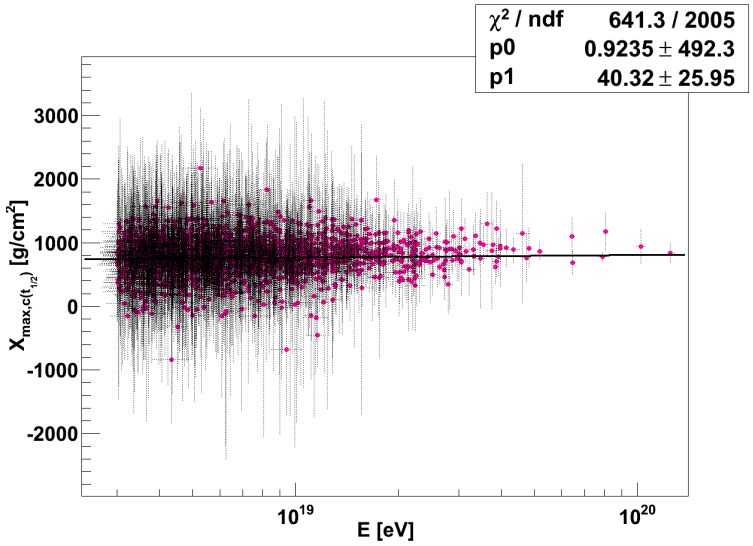

Figure 4.3: The energy dependency of the calculated X_{max} using the SD parameter $t_{1/2}$.

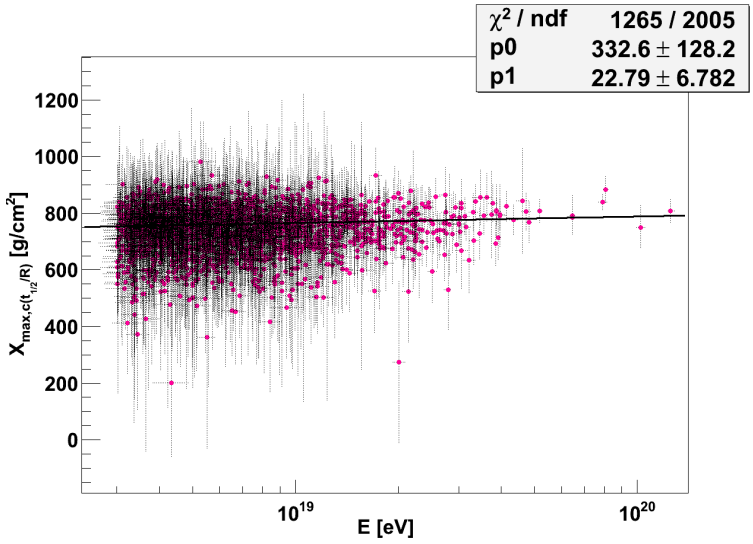

Figure 4.4: The energy dependency of the calculated X_{max} using the combination of SD parameters $t_{1/2}$/R.

value, within the uncertainty of one σ. The uncertainties on $X_{max,c(t_{1/2}/R)}$ are still large due to the calculation.
Again, because of the weak correlations, the calculated $X_{max,c(t_{1/2}/R)}$ from the SD data is not as reliable as hoped for and it does not work to get an accurate

X_{max} out of the SD data while working with this method.
This is why further research is neccessary to be able to say if calculating a X_{max} from SD data is reliable.
No correction for the opening angle of the telescope has been taken into account in this study as it has been done for example for the literature value of the elongation rate. It might be interesting to look into this in further research.

Appendix A

Used selection criteria

A.1 List of FD selection criteria

Description	Code: theRecEvent->GetFDEvents()->at(FD_Eye)->
Reconstruction level	GetRecLevel() >= 10
Number degrees of freedom	GetFdRecShower()->GetGHNdf()>=1
Distance shower axis - FD	GetFdRecGeometry()->GetStationAxisDistance() < 2000.0
Cherenkov fration	GetFdRecShower()->GetCherenkovFraction() < 50
LIDAR	HasLidarData(FD_Eye) == 0 GetLidarData(FD_Eye)->GetCloudCoverage() > 0.
VAOD	GetDetector()->GetVAODAtReferenceHeight(FD_Eye)>=0.06
X_{max} in field of view	GetFdRecShower()->IsXmaxInFOV(100)
χ^2/ndf of GH	$\frac{\text{GetFdRecShower()->GetGHChi2()}}{\text{GetFdRecShower()->GetGHNdf()}}$<1.4625

A.2 List of SD selection criteria

Description	Code: theRecEvent->GetSDEvent()->
Reconstruction level	GetRecLevel()>= 4
Zenith angle θ	$\frac{\text{GetSdRecShower()->GetZenith()}}{\text{TMath::Pi()*180}} < 60.$
Energy	GetSdRecShower()->GetEnergy() > 3e18 $\frac{\text{GetSdRecShower()->GetEnergyError()}}{\text{GetSdRecShower()->GetEnergy()*100}} < 13$
Number degrees of freedom (LDF)	GetSdRecShower()->GetLDFNdof()>=1
Number degrees of freedom (Angle)	GetSdRecShower()->GetAngleNDoF()>=1
6T5 trigger	Is6T5()
More than 5 stations triggered	GetNumberOfCandidates()>5
Risetime $t_{1/2}$	GetRiseTimeResults()->GetRiseTime1000() > 0 GetRiseTimeResults()->GetRiseTimeNDF()>=1 $\frac{\text{GetRiseTimeResults()->GetRiseTimeChi2()}}{\text{GetRiseTimeResults()->GetRiseTimeNDF()}} < 10$
χ^2/ndf of LDF and AF	$\frac{\text{GetSdRecShower()->GetLDFChi2()}}{\text{GetSdRecShower()->GetLDFNdof()}} < 3.05$ $\frac{\text{GetSdRecShower()->GetAngleChi2()}}{\text{GetSdRecShower()->GetAngleNDoF()}} < 5.775$

Appendix B

Uncertainty propagation and the estimation of expected slopes

B.1 Uncertainty propagation

The uncertainties in this study are calculated as follows:

$$f = f(x_1, x_2, ..., x_n)$$

$$(\sigma_f)^2 = \sum_{i=1}^{n} (\frac{\partial f}{\partial x_i})^2 \cdot \sigma_{x_i}^2$$

B.2 Estimation of expected slopes for the combination of two parameters

Considering two given functions

$$x = a \cdot (r - r_0) + x_c$$

$$x = b \cdot (t - t_0) + x_c$$

$$x = c \cdot \left(\frac{t}{r} - \left(\frac{t}{r}\right)_0\right) + x_c$$

This substitution simplifies the following analysis:

$$y = x - x_c = x - 750$$

$$y = a \cdot (r - r_0) \tag{B.1}$$

$$y = b \cdot (t - t_0) \tag{B.2}$$

$$y = c \cdot \left(\frac{t}{r} - \left(\frac{t}{r}\right)_0\right) \tag{B.3}$$

Putting equations B.1 ad B.3 together yields:

$$a \cdot (r - r_0) = c \cdot \left(\frac{t}{r} - \left(\frac{t}{r}\right)_0\right)$$

Multiplying with r/c on both sides yields:

$$\frac{a \cdot r}{c} \cdot (r - r_0) = t - \left(\frac{t}{r}\right)_0 \cdot r$$

$$\frac{a \cdot r}{c} \cdot (r - r_0) + \left(\frac{t}{r}\right)_0 \cdot r = t = \frac{y}{b} + t_0$$

$$y = \frac{a \cdot b}{c} \cdot r \cdot (r - r_0) + \left(\frac{t}{r}\right)_0 \cdot r \cdot b - t_0 \cdot b$$

Because of r(r-r_0) = r^2-r · r_0 =(r-r_0)^2 + r_0 (r - r_0) this leads to

$$y = \frac{a \cdot b}{c} \cdot (r - r_0)^2 + \frac{a \cdot b}{c} \cdot r_0 \cdot (r - r_0) + \left(\frac{t}{r}\right)_0 \cdot b \cdot (r - r_0) + \left(\frac{t}{r}\right)_0 \cdot b \cdot r_0 - t_0 \cdot b$$

$$y = \frac{a \cdot b}{c} \cdot (r - r_0)^2 + \left(\frac{a \cdot b}{c} \cdot r_0 + \left(\frac{t}{r}\right)_0 \cdot b\right)(r - r_0) + \left(\frac{t}{r}\right)_0 \cdot b \cdot r_0 - t_0 \cdot b \tag{B.4}$$

Because $(r - r_0)$ is relatively small, the term including $(r - r_0)^2$ in equation B.4 can be neglected. This leads to

$$\left(\frac{a \cdot b}{c} \cdot r_0 + \left(\frac{t}{r}\right)_0 \cdot b\right) = a$$

$$c = \frac{a \cdot b \cdot r_0}{a - \left(\frac{t}{r}\right)_0} \cdot b \tag{B.5}$$

The term that is independen of $(r - r_0)$ in equation B.4 is expected to be approximately zero because of equation B.1:

$$\left(\frac{t}{r}\right)_0 \cdot b \cdot r_0 - t_0 \cdot b = 0$$

$$\left(\frac{t}{r}\right)_0 \cdot b \cdot r_0 = t_0 \cdot b$$

$$\left(\frac{t}{r}\right)_0 = \frac{t_0}{r_0}.$$

Using the values a = -28.57, b = 7.92, r_0 = 8.35, t_0 = 244.73 and $(t/r)_0$ = 28.69, the value of the expected slope is according to equation B.5 c = 7.4. Because $\frac{t_0}{r_0}$ = 29.3 there is a stronger correlation when using the parameter combination.

Bibliography

[1] T. Stanev, *High Energy Cosmic Rays*, second edition, 2010

[2] P. Sommers, *The Logic of the Auger Hybrid Design*, GAP_97_002

[3] G. van Aar, *A study of composition and anisotropy of cosmic rays using the shape of the air shower front*, http://www.ru.nl/publish/pages/557611/thesis_gva.pdf

[4] R. Ulrich, *Measurement of the Proton-air Cross Section using Hybrid Data of the Pierre Auger Observatory*, 2008

[5] F. Nerling, GAP2005-063

[6] L. Perrone, S. Petrera, F.Salamida, *Gaisser-Hillas profiles and FD Simulation*,ÂŞ GAP2005-087, 2005

[7] B. Dawson, GAP1996-017

[8] G. van Aar, GAP2011-026

[9] E. Parizot, I. Lhenry, D. Allard, P. Ghia, G. Navarra, *First steps towards the definition of a "quality trigger" (T5) for the SD acceptance calculations*, GAP2004_023

[10] D. Veberič, M. Roth, H. Dembinski, [?], Version 0.8, 2010

[11] K. Greisen, *End to the Cosmic-Ray Spectrum?*, Physical Review Letters, Volume 16, Issue 17, 25/04/1966

[12] www.auger.org

[13] http://www.auger.org/technical_info/pdfs/icrc2003/lateral_distribution.pdf

[14] http://www.ung.si/public/pao/bibl/elba_2003_mussa.pdf

[15] Pedro Facal San Luis, *The distribution of shower maxima of UHECR air showers*, ICRC2011

[16] P. Auger, *Extensive Cosmic-Ray Showers*, Rev. Mod. Phys., Vol. 11, p. 288-291 (1939)

[17] J. Lindsey, *Evidence for a primary cosmic-ray particle with energy* 10^{20} *eV*, Physical Review Letters, 15 February 1963, Volume 10, Number 4

[18] Pierre Auger Collaboration, *Measurement of the energy spectrum of cosmic rays above* 10^{18} *eV using the Pierre Auger Observatory*, Physics Letters B, 685 (4-5), p. 239-246, Mar 2010